NAVAL POSTGRADUATE SCHOOL

MONTEREY, CALIFORNIA

THESIS

TUNABLE BANDWIDTH QUANTUM WELL INFRARED PHOTO DETECTOR (TB-QWIP)

by

Mihail Giannopoulos

December 2003

Thesis Advisor:	Gamani Karunasiri
Second Reader:	James Luscombe

THIS PAGE INTENTIONALLY LEFT BLANK

REPORT DOCUMENTATION PAGE

Form Approved OMB No. 0704-0188

1. AGENCY USE ONLY ***(Leave blank)***	**2. REPORT DATE** December 2003	**3. REPORT TYPE AND DATES COVERED** Master's Thesis

4. TITLE AND SUBTITLE Tunable Bandwidth Quantum Well Infrared Photo Detector (TB-QWIP)

5. FUNDING NUMBERS

6. AUTHOR (S) Mihail Giannopoulos

7. PERFORMING ORGANIZATION NAME(S) AND ADDRESS(ES)
Naval Postgraduate School
Monterey, CA 93943-5000

8. PERFORMING ORGANIZATION REPORT NUMBER

9. SPONSORING / MONITORING AGENCY NAME(S) AND ADDRESS(ES)
N/A

10. SPONSORING/MONITORING AGENCY REPORT NUMBER

11. SUPPLEMENTARY NOTES The views expressed in this thesis are those of the author and do not reflect the official policy or position of the U.S. Department of Defense or the U.S. Government.

12a. DISTRIBUTION / AVAILABILITY STATEMENT
Approved for public release; distribution is unlimited

12b. DISTRIBUTION CODE

13. ABSTRACT ***(maximum 200 words)***

In this thesis a tunable bandwidth quantum well photo-detector (TB-QWIP) is fabricated and experimentally characterized. The designed detector is based on the Stark effect with two quantum step wells arranged opposite to each other to simultaneously achieve both blue- and red-shift of the absorption peak for either direction of the bias.

The characterization of the TB-QWIP is based on absorption measurement with Fourier Transform Infra Red (FTIR) spectroscopy, current versus applied voltage (I-V) measurement with a semiconductor parameter analyzer, and photocurrent spectroscopy. The measured IR absorption peaks found at room temperature $8.8\,\mu\mathrm{m}$ and $10.0\,\mu\mathrm{m}$ are in good agreement with designed values. The dark current of the test detector was found to be 10^{-9} A and a background photocurrent was found to be 700×10^{-9} A at -4 V bias at 10 K. The background-limited performance of the device was found to be at 60 K. The peak responsivity of the detector was 0.39 A/W at 8.2 μm. The maximum normalized detectivity under background limited conditions D^*_{BLIP}, was calculated to be $3.5 \times 10^{11}\,\mathrm{cm}\sqrt{\mathrm{Hz}}/W$. The bandwidth of the detector tuned with bias from 1.8 μm at -1 V to 2.7 μm at -4 V, which amounts to 50% higher than the original width.

Further tuning of TB-QWIP parameters based on the analysis of this thesis hold promise for 100% increase of peak width by an applied bias.

14. SUBJECT TERMS Tunable Bandwidth Quantum Well Infrared Photo-detector (TB-QWIP); Absorption; FTIR; I-V characteristics; Photo current; Responsivity; Dedectivity; Background Limited; Tunability;	**15. NUMBER OF PAGES** 64
	16. PRICE CODE

17. SECURITY CLASSIFICATION OF REPORT	**18. SECURITY CLASSIFICATION OF THIS PAGE**	**19. SECURITY CLASSIFICATION OF ABSTRACT**	**20. LIMITATION OF ABSTRACT**
Unclassified	Unclassified	Unclassified	UL

NSN 7540-01-280-5500 **Standard Form 298 (Rev. 2-89) Prescribed by ANSI Std. 239-18**

THIS PAGE INTENTIONALLY LEFT BLANK

Approved for public release; distribution is unlimited.

TUNABLE BANDWIDTH
QUANTUM WELL INFRARED PHOTO DETECTOR (TB-QWIP)

Mihail Giannopoulos
Lieutenant Colonel, Hellenic Air Force
B.E., Hellenic Air Force Academy, 1987

Submitted in partial fulfillment of the
requirements for the degree of

MASTER OF SCIENCE IN APPLIED PHYSICS

from the

NAVAL POSTGRADUATE SCHOOL
December 2003

Author: Mihail Giannopoulos

Approved by: Gamani Karunasiri
Thesis Advisor

James Luscombe
Co-Advisor

James Luscombe
Chairman, Department of Physics

THIS PAGE INTENTIONALLY LEFT BLANK

ABSTRACT

In this thesis a tunable bandwidth quantum well photo-detector (TB-QWIP) is fabricated and experimentally characterized. The designed detector is based on the Stark effect with two quantum step wells arranged opposite to each other to simultaneously achieve both blue- and red-shift of the absorption peak for either direction of the bias.

The characterization of the TB-QWIP is based on absorption measurement with Fourier Transform Infra Red (FTIR) spectroscopy, current versus applied voltage (I-V) measurement with a semiconductor parameter analyzer, and photo current spectroscopy. The measured IR absorption peaks found at room temperature 8.8 μm and 10.0 μm, are in good agreement with designed values. The dark current of the test detector was found to be 10^{-9} A and a background photocurrent was found to be 700 x 10^{-9} A at -4 V bias at 10 K. The background-limited performance of the device was found to be at 60 K. The peak responsivity of the detector was 0.39 A/W at 8.2 μm. The maximum normalized detectivity under background limited conditions D^*_{BLIP}, was calculated to be 3.5 x 10^{11} $\mathrm{cm}\sqrt{\mathrm{Hz}}/W$. The bandwidth of the detector tuned with bias from 1.8 μm at -1 V to 2.7 μm at -4 V, which amounts to 50% higher bandwidth than the original.

Further tuning of TB-QWIP parameters based on the analysis of this thesis hold promise for 100% increase of peak width by an applied bias.

THIS PAGE INTENTIONALLY LEFT BLANK

TABLE OF CONTENTS

LIST OF FIGURES

LIST OF TABLES

THIS PAGE INTENTIONALLY LEFT BLANK

ACKNOWLEDGEMENTS

I would like to thank Professor Gamani Karunasiri for his outstanding teaching and guiding method and Professor James Luscombe for his invaluable introduction to the Quantum world.

Thank to all of my Professors at the Naval Postgraduate School who have shown me the beauty of knowledge, uncovered the principles behind state of the art technology and broadened my field of view in today’s high and wide knowledge-demanding environment.

Furthermore I want to thank my wife and my three sons, for their understanding and support. They made this thesis possible.

THIS PAGE INTENTIONALLY LEFT BLANK

I. INTRODUCTION

A. SEMICONDUCTORS AND INFRARED APPLICATIONS

1. Optical Properties of Semiconductors

The solution of Schrödinger's equation for an electron in an atom (electron in a potential well), gives **quantized energy levels**. Electrons in a solid have a range or band of available energy levels, called **energy bands**. Available energies are separated by energy gaps. The last occupied band by electrons is called the valence band, and the first non-occupied band is called the conduction band. The separation of the valence band and the conduction band called the **band gap** of the material. In a semiconductor the band gap is the minimum energy necessary for an electron to transfer from the valence band into the conduction band, where it moves more freely. Semiconductors can absorb and emit photons by undergoing transitions between the conduction and valence band. The **absorption** of a photon can create electron hole pairs, which alter the electrical properties of semiconductors.

Photo-detectors are devices used to sense incident radiation. Semiconductor photo detectors can convert an optical signal to an electrical signal. Within the last twenty years a new approach to semiconductor development was established that allows researchers to create semiconductor hetero-structures. Semiconductor growth methods such as molecular beam epitaxy (MBE), and metal organic chemical vapor deposition (MOCVD) can make materials, one atomic monolayer at a time. These layers are so thin that the continuous energy levels found in bulk

material become **discrete energy levels** within these thin layers. Using these techniques, semiconductors can be man made to have optical and electrical properties and characteristics that are desirable for optical-radiation detectors. This approach to making new materials is known as **band gap engineering** (Capaso et al 1983; Ferry 1985). The bandgap-engineering of semiconductors and the development of quantum mechanical tools provide an opportunity to fabricate quantum well infrared photo-detectors (QWIP) with novel properties (Levine 1993).

2. Infrared Applications

Wavelength is an important parameter of light, which enables us to classify radiation into categories, such as infrared, visible, or microwave as illustrated in Figure 1.

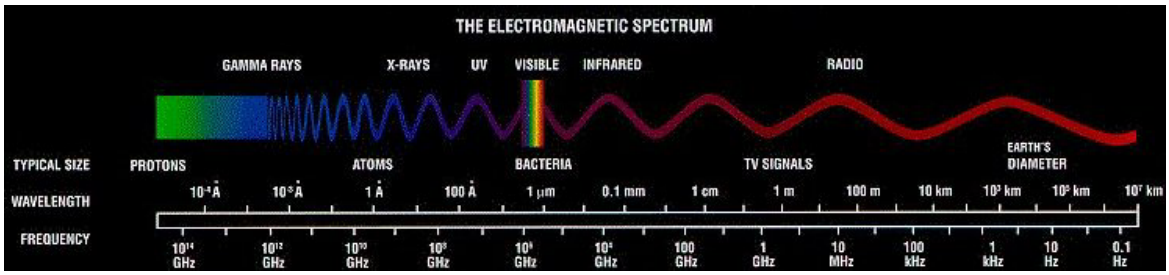

Figure 1. Wavelength classification of electromagnetic spectrum.

Infrared light shows us the heat radiated by the world around us. Middle wavelength infrared (MWIR) and long wavelength infrared (LWIR) detection in particular is very important for a wide range of applications due to the 3-5μm and 8-14μm atmospheric windows. Another important reason is due to the glowing radiation peak of materials at room

temperature around 10 μm, and the effectiveness of 3-5μm detection in tropical environments. Nowadays infrared detection has the following scientific, commercial, and military applications:

- Scientific:
  - Universe exploration and extraterrestrial search
  - Tumor characterization and determination of cancer cells "tone"
  - Accurate non-invasive determination of substance temperature
  - Animal studies
  - Weather prediction
  - Gradual long-term evaluation of ecosystem dynamics
  - Humidity concentration, and ocean currents observations (prediction of natural impending phenomena or disasters)
  - Ozone and greenhouse gas monitoring
  - Volcano eruptions detection
  - Historical objects preservation and restoration
  - Art authentication and valuation
  - Law enforcement
  - Fire fighting

- Commercial:
  - Security and Surveillance
  - Mechanical systems maintenance
  - Electrical systems inspection
  - Food unwholesome products rapid detection

- Soil status or stressed vegetation fields determination (of normal and contaminated parts)
- Navigation through thick fog and clouds
- Structure heat lost detection
- Process control, quality assurance and product monitoring
- Design validation, non destructive testing, and thermal analysis
- Biometric Monitoring
- Accident Avoidance Systems and Intelligent Traffic Systems

❖ Military:

- Remote sensing, satellite imaging and reconnaissance
- Unmanned ground, underwater, air vehicles (UGVs, UUVs,UAVs)
- Search and rescue, combat search and rescue (SAR, CSAR)
- Camouflage-concealment-deception (CCD)
- Terrain analyzing and planning
- Air-route preparation and weapons-delivering
- Night vision and night sighting
- Mine detection
- Forward looking infrared (FLIR)
- Low Altitude Navigation and Targeting Infrared for Night (LANTIRN)
- Laser target designation, ranging and spot tracking (LST)
- Infrared search and track (IRST)

- Optical processing for radar and sonar signals
- TV and IR precision munitions guiding and homing
- Laser warning receiving and laser communicating
- IR signatures suppressing,
- Tactical battle picturing and Situation awareness (SA)
- IR electronic-protection-measurements (EPM) and IR jamming
- Tactical automated security systems (TASS)
- Blended visible-IR imaging, aiming and targeting
- Missile seekers and Smart Munitions guiding

A great example of the importance of infrared detection is the Space Infrared Telescope Facility (SIRTF) launched from Cape Canaveral Air Force Station in Florida on August 25 2003. During its 2.5-year mission, SIRTF will obtain images and spectra by detecting the infrared energy, or heat, radiated by objects in space between wavelengths of 3 and 180 microns.

From the military point of view, it is the author’s strong belief that advanced IR detectors and passive or low observable technology is a contemporary need in an unpredictable combat theatre while at the same time infrared detection itself is a counter stealth challenge.

THIS PAGE INTENTIONALLY LEFT BLANK

B. QUANTUM WELL INFRARED PHOTODETECTORS (QWIP)

1. Quantum Well Structures

Quantum well detectors operate by detecting the optical energy from a heated object, instead of relying directly on the transfer of heat energy (like thermal detectors do). A quantum well can be visualized as a potential well whose electrons and holes are trapped, as illustrated in Figure 2. The bound electrons in the quantum well absorb the incident light. The detection process involves measuring the absorption and converting it to an electrical signal. Conventional **inter-band** optical absorption involves photo-exciting carriers across the band gap E_g. Incident light with energy corresponding to the energy separation between two states results in a sharp absorption.

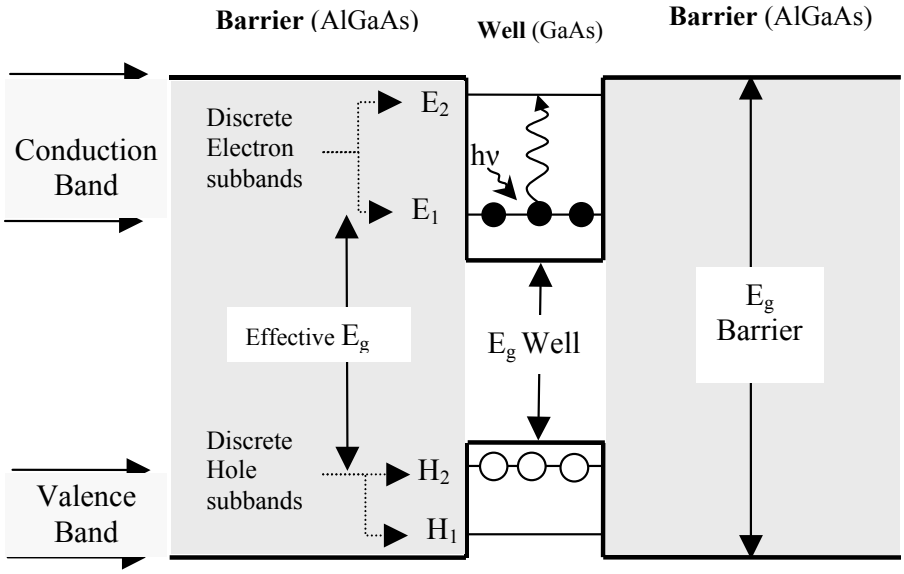

Figure 2. Band structure of a quantum well. Inter-sub-band absorption between electron levels E_1 and E_2 (*bound to bound* transition) or hole levels H_1, H_2.

When the electrons in a quantum well are disturbed by incident light, they can be ejected out of the well. If an external voltage is applied these electrons produce a photocurrent. The current produced is proportional to the photon flux incident upon the quantum well. By measuring the current, a quantum well photo-detector (QWIP) can tell how much light comes from various sources at the scene being imaged. The QW structure parameters can be designed so that the photo-excited carriers can escape from the potential wells and be collected as photocurrent. The longer the wavelength of light, the less energy the light has to give the electrons and the colder the detector must be to avoid excessive thermal excitations. The detection of long wavelength infrared radiation around 10 μm requires a semiconductor having relatively small band gap (about 0.1 eV). It is very difficult and expensive to grow such semiconductors, to process and to fabricate materials that naturally have “loose” electrons, what are called “low band-gap materials”. To overcome these difficulties of low band gap materials, it is possible to employ large band gap materials for LWIR detection by using **inter-sub-band** absorption, involving transition of carriers within the same band (Coon and Karunasiri 1984, and 1985, West 1985, Levine 1987). The band gap discontinuity of two materials creates quantized sub-bands in the potential wells associated with conduction band or valence band, as shown in Figure 2.

By sandwiching in series, a thin layer of narrow band gap material, between two usually thicker layers of a wider gap material, for example, GaAs between $Al_xGa_{1-x}As$ a multiple quantum well (MQW) structure may be formed as shown in Figure 3.

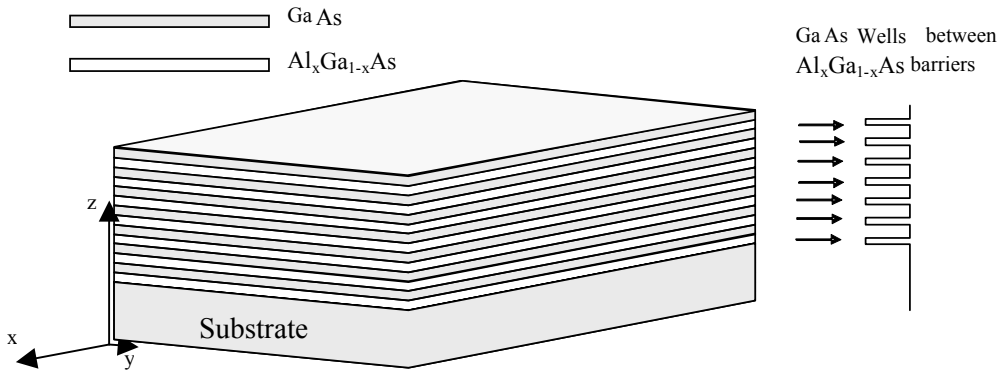

Figure 3. A multiple quantum well structure made of GaAs and $Al_xGa_{1-x}As$ on a GaAs substrate. Electrons are free to move in the x-y plane but are facing barriers and wells in the growth z direction.

The effect of the potential wells involving inter-sub-band transitions is to reduce the number of degrees of freedom of free carriers inside the well of the narrow gap material. As illustrated in Figure 3, carriers are free to move in the x-y plane, but they are facing energy barriers and wells in z direction. A well is regarded as being narrow if its width is less than the electron de Broglie wavelength. In such a case, the permissible electron energies are quantized along the growth direction. The advantages of using inter-sub-band transitions in QWIP detectors based on $Al_xGa_{1-x}As$, compared with detectors using transitions across the band gap like mercury cadmium telluride HgCdTe (MCT), include the mature AlGaAs growth

and process technologies, which lead to high uniformity, excellent reproducibility, and thus large-area, low-cost staring arrays (Rogalski 2003). The ability to accurately control the band structure, and hence spectral response, allows integrated multi spectral and high-speed IR detectors. In addition, inter-sub-band transitions in quantum wells can be used for fabrication of high-speed infrared modulators due to the shift of absorption wavelength with bias (Karunasiri 1990) and lasers (Levine 1993). The energy levels in the quantum well are determined by the thickness and depth of the wells (Levine 1993). The bandgap of $Al_xGa_{1-x}As$ and hence the depth of the wells can be changed by varying the Al molar ratio x. The width and the depth of the well can be chosen, such that, excitation happens from the bound ground state to continuum states (Coon and Karunasiri 1984, and Hasnain *et al* 1989), as illustrated in Figure 4 for a MQW structure under an applied bias.

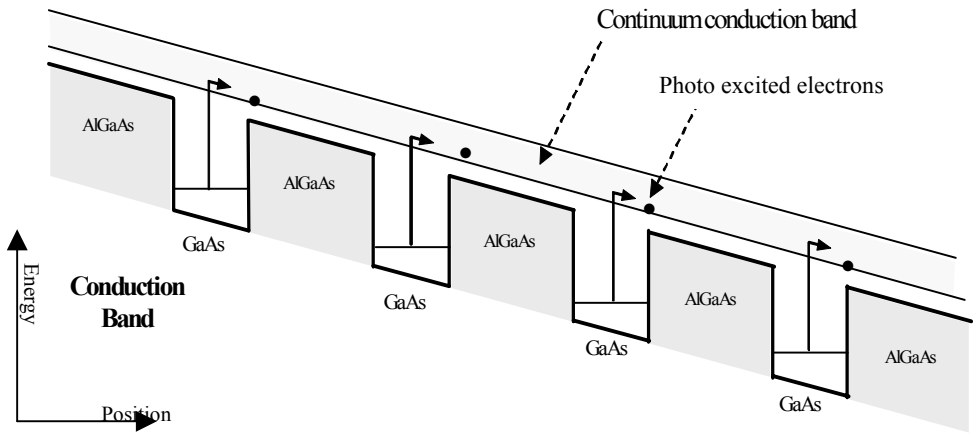

Figure 4. Bound-to-continuum transitions under applied bias.

The bound to continuum absorption mechanism is the excitation of an electron from the doped quantum well ground state in the conduction band to the continuum states in the same band. The advantage of the *bound to continuum* transitions is that the photo-excited electrons escape from the well to the continuum states without tunneling. Other QWIP configurations have been reported based on transitions from *bound to extended states* (Levine, 1991) and *bound to miniband* states (Yu, 1991). Both configurations provide good detection performance because in the designs, electrons in the ground state do not flow in response to the bias, while excited electrons yield photocurrent under low bias. Another quantum well design, based on transitions from *bound-to-quasibound* states (Gunapala *et al* 1995), places the first excited state exactly at the well top as shown in Figure 5.

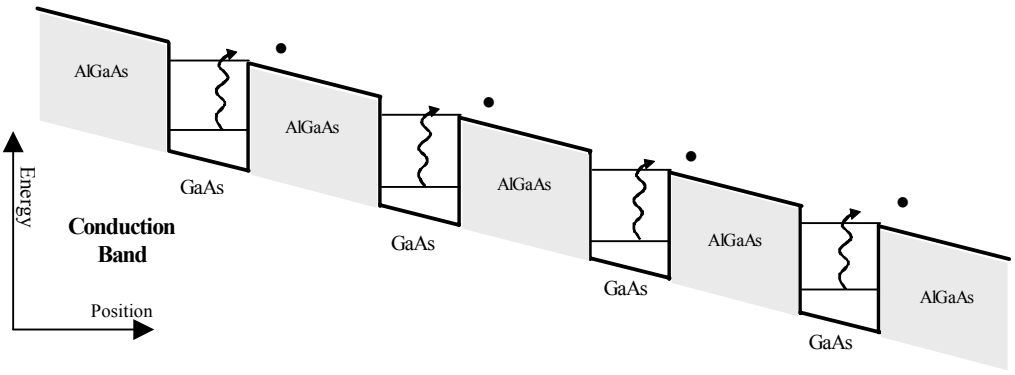

Figure 5. Bound-to-quasibound electron transitions in MQW.

Bound-to-quasibound quantum well design further improves the detection performance of a QWIP detector, by reducing the dark current and so, allows higher temperature detector operation.

2. Tunable Bandwidth QWIP (TB-QWIP)

A tunable bandwidth quantum well infrared photo-detector is based on the energy shift of the inter-sub-band transition energy under an applied electric field. This shift is called the *Stark effect*. In a square quantum well, biased with low electric field strength, the *Stark effect* is small (Martinet *et al* 1992). The reason is that all the energy states will shift in the same direction in a symmetric well. In a step quantum well, which is consists of a small well inside a big well, the *Stark effect* or the energy shift of the inter-sub-band transition under an applied field is large due to the asymmetry of the structure (Yuh 1989, and Martinet *et al* 1992). A step well can be designed so that the Stark shift can take place from the ground state to the first quasi-bound state. The absorption peak of the well is sensitive to the direction of the applied field (Mii, 1988). By changing the direction of the field, the absorption peak can be either blue or red shifted. Taking advantage of the ability to shift absorption peaks in a step well with an applied bias it is possible to broaden the absorption peak width, if two identical step wells are arranged opposite to each other to form a *mirror step well* as shown in Figure 6.

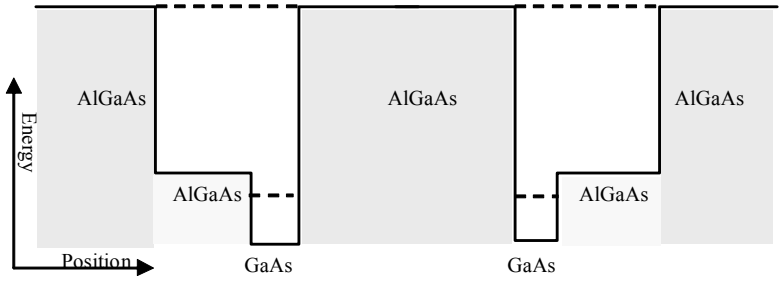

Figure 6. Mirror step quantum well structure of $Al_xGa_{1-x}As$.

With no electric field applied, this structure has one sharp absorption peak because both step wells have identical sub-band separation. An applied electric field will simultaneously blue- and red-shift the absorption peaks of the mirror step wells and hence broaden the combined absorption peak width. This effect can be utilized to fabricate voltage tunable bandwidth quantum well infrared photo-detectors.

3. Tunable QWIP

In the past decade, there has been an extensive research effort to achieve electronically **tunable** wavelength QWIP detectors to improve the signal to noise ratio and to overcome specific obscurants for identifying chemical agents and materials. The advantages of tunable detectors are that they are lightweight, flexible, fast, multi objective, and multi function, and they resist jamming detection. Tunable QWIPs have been proposed using coupled QWs (Choi *et al* 1989), graded barriers (Levine 1990), or asymmetric step wells (Martinet *et al* 1992). Also, broadened spectral QWIP detectors can be constructed by stacking different quantum wells in a repeating sequence (Bandara 1997, 2001). In parallel, during the past few years there is an effort to achieve electronically **tunable bandwidth** quantum well infrared photo detectors (Choi K. K. [1]), or tunable bandwidth quantum dot infrared photo-detectors (QDIP), (S. Krishna et al 2002)[2], as a hyper

[1] For more information, refer to "Agile and versatile infrared technology based on QWIPs": http://www.asc2002.com/summaries/j/JP-04.pdf (Oct. 2003)

[2] For more information, refer to: http://www.ieee.org/organizations/pubs/newsletters/leos/feb02/dot.html#hotfig1 (Oct. 2003)

spectral contrivance with additional multifunction advantages. Very fast (in order of 10ps) quantum well spatial light modulators (Karunasiri 1990), combined with an FPA-TB-QWIP detectors can be a powerful Hyper Spectral Imaging (HSI) instrument to detect targets that are masked from conventional radars. Also TB-QWIP combined with tunable laser source can be a powerful active hyper-spectral search track and ranging system.

C. PURPOSE OF THIS THESIS

Today's infrared detectors must be modular re-configurable and flexible in general, with capabilities across the "full spectrum" of operations. A potential solution for the demand of flexible broadband detector is a tunable bandwidth quantum well infrared photo detector (TB-QWIP). The purpose of this thesis is the analysis and characterization of a fabricated TB-QWIP, which is theoretically proposed by Konukbay (2002). The fabricated detector is based on mirror step wells as shown in Figure 7.

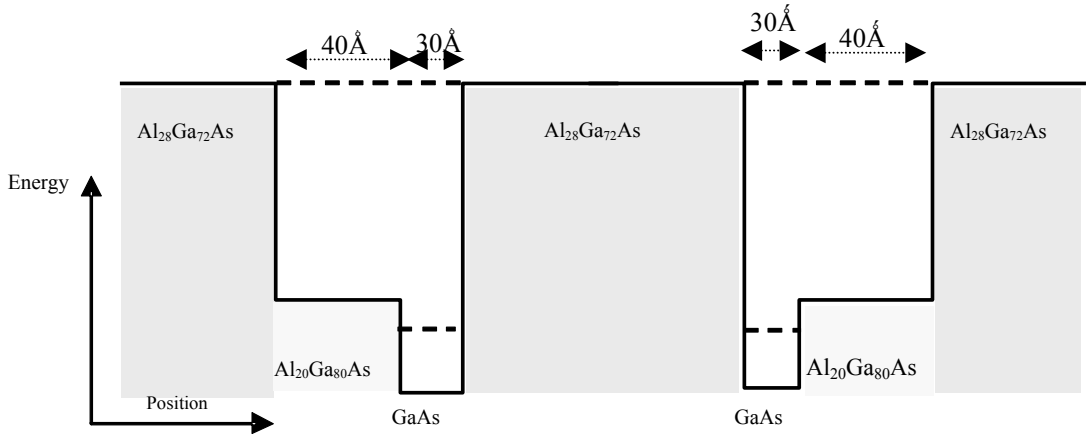

Figure 7. Fabricated quantum well structure of $Al_xGa_{1-x}As$.

The ability to tune the bandwidth of the detector is based on the linear Stark effect in an asymmetric quantum well (Yuh 1989) for the ground state to the first quasibound state. The detector has two identical step-wells arranged opposite to each other, which can both blue- and red-shift the absorption peak for either direction of the bias. The bandwidth of the response of the detector should be proportional to the applied bias due to the linear Stark effect. A period of the structure is schematically shown in Figure 8. *It* consists of 20 periods of $Al_{28}Ga_{72}As$ - $Al_{20}Ga_{80}As$ - GaAs - $Al_{28}Ga_{72}As$ - GaAs - $Al_{20}Ga_{80}As$ - $Al_{28}Ga_{72}$. The GaAs well, is doped with Si, 10^{18} cm^{-3}. The epitaxial wafer data are given in appendix 1.

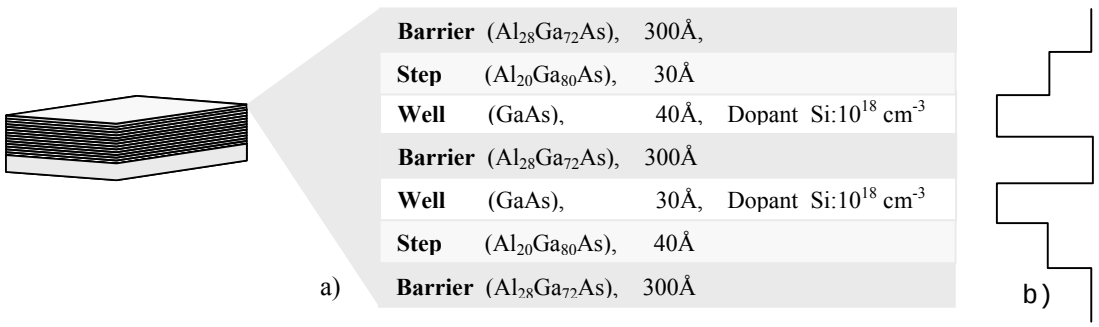

Figure 8. a) One period of the fabricated MQW.
b) The corresponding energy diagram.

The details of the design of the structure can be found in (Konukbay 2002). The grown quantum well structure is slightly different from the one shown in Figure 7 where the two wells have the same thickness.

The Energy diagram and energy levels of an unbiased period of the fabricated *mirror-like step* quantum well structure is illustrated in Figure 9.

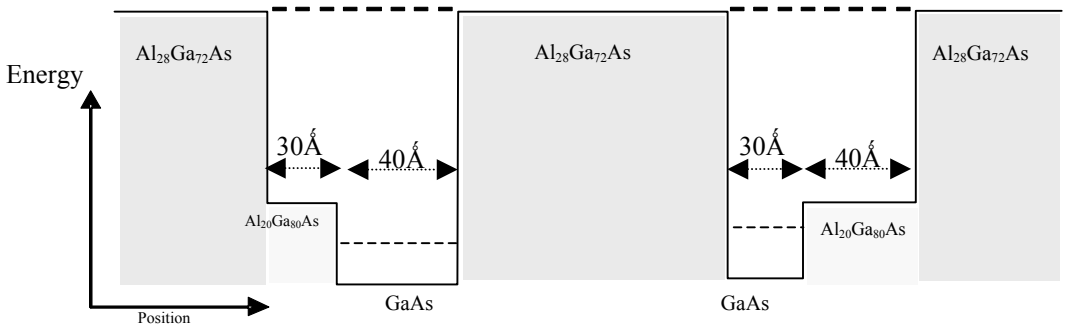

Figure 9. Energy levels and one period of the fabricated *mirror-like step* well structure.

The characterization of the detector will be based on measurement and analysis of the following:

- Absorption measurements
- Current versus voltage (I-V) characteristics and
- Photocurrent spectroscopy

The thesis is organized as follows. Chapter I, gives the introduction followed by the design of the quantum well structure. Chapter II describes the absorption measurements using Fourier transform infrared (FTIR) spectroscopy. Chapter III describes the I-V characteristics of the detector as a function of operating temperature. These characteristics are measured under dark and open to

background, to determine the background limited performance of the detector. Chapter IV presents the photocurrent measurement to determine the responsivity and to demonstrate the bandwidth tunability of the detector. Finally, in Chapter V the conclusion of the thesis is given with recommendations for future research.

THIS PAGE INTENTIONALLY LEFT BLANK

II. ABSORPTION

A. INTRODUCTION

1. Fourier Transform Infrared (FTIR) Spectroscopy

An FTIR spectrometer typically uses a Michelson interferometer and passes the recombined beam of light through the sample after a path difference is introduced. The Michelson interferometer consists of two mutually perpendicular front-coated mirrors, one of which can be moved along the axis perpendicular to its plane, as schematically illustrated in Figure 10.

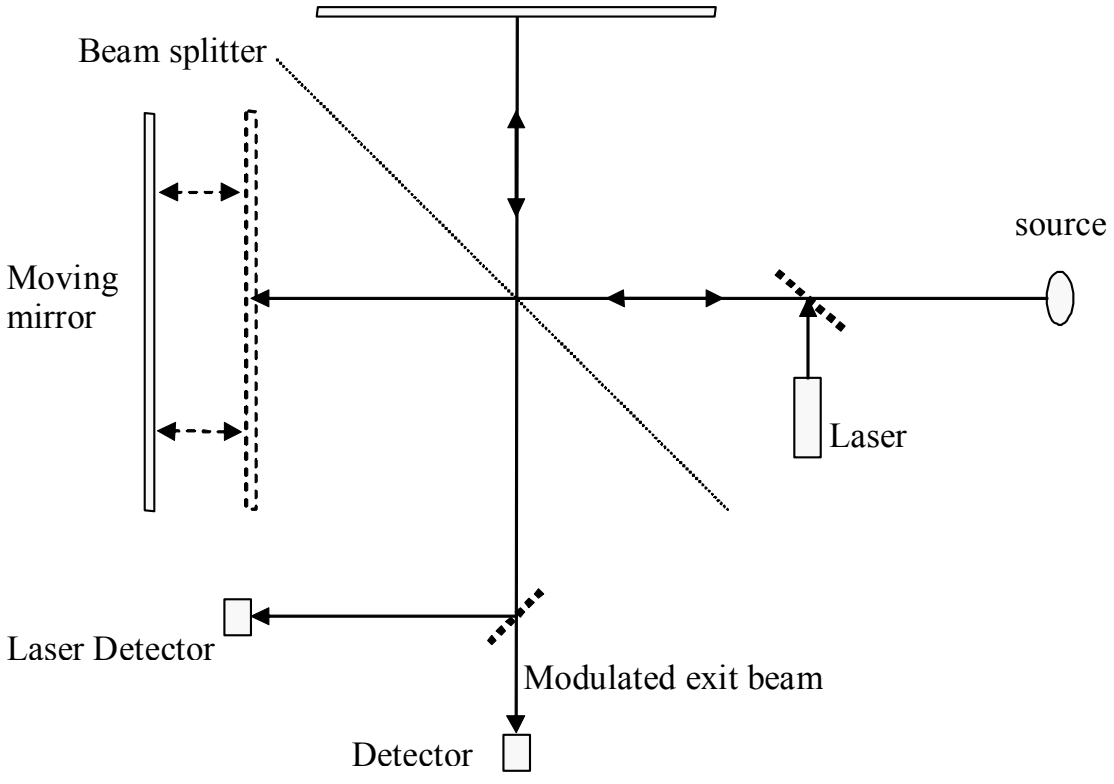

Figure 10. A schematic diagram of the FTIR interferometer.

The position of the moving mirror is usually monitored with a laser beam that also passes through the interferometer. **The sample absorbs** all the different wavelengths characteristic of its spectrum, and this subtracts specific wavelengths from the interferogram. A detector in the FTIR spectrometer senses variation in energy versus time for all wavelengths simultaneously. The laser beam is superimposed to provide a reference for the instrument operation. The output of the detector is digitized, and a computer program does the Fourier transform for *every point* in the interferogram instantaneously. The computer program converts intensity versus time spectrum into intensity versus frequency spectrum and displays the results.

2. Inter-sub-band Transition Measurement with FTIR

Inter-sub-band transitions in quantum wells can be conveniently measured using FTIR spectroscopy. The *bound-to-bound* transitions are typically narrow band and can be studied by placing the sample at Brewster's angle to the infrared beam (Levine 1993). The Brewster's angle has the advantage that there is no reflection of the incident beam, if the polarization of light is in the plane of incidence. However the absorption peak is weak due to the relatively small thickness of the multiple quantum well structure and only one pass of the beam through the structure occurs as shown in Figure 11.

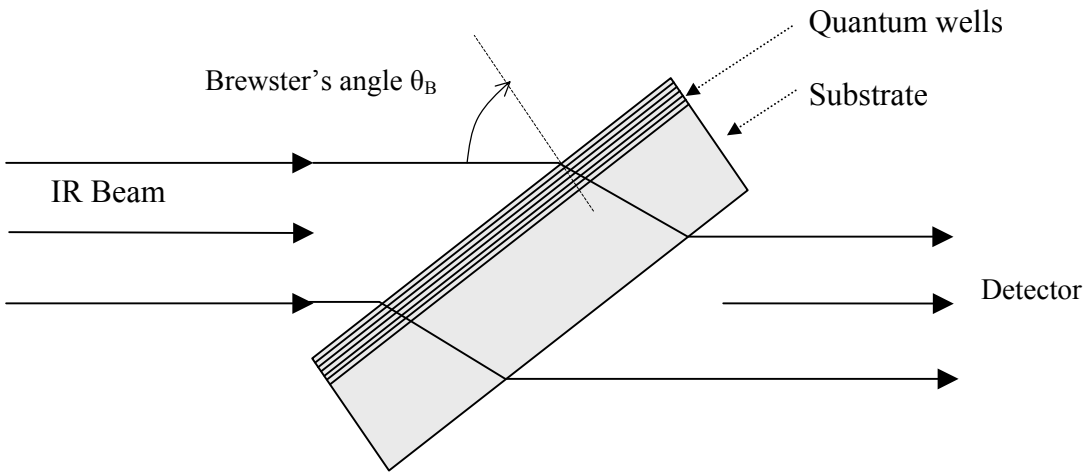

Figure 11. Sample arrangement in Brewster's angle θ_B relative to the IR beam. This geometry is typically used in the study *of bound-to-bound transitions.*

The *bound to continuum* transitions generally have broader absorption peaks and the magnitude of the absorption at a given wavelength is smaller than the bound-to-bound transitions. In order to overcome this problem a waveguide

structure (Levine 1993) is used to have multiple passes of the IR beam through the quantum wells as illustrated in Figure 12. The *mirror step* well, from now on will also be referred as tunable bandwidth quantum well infrared photo detector (TB-QWIP) structure.

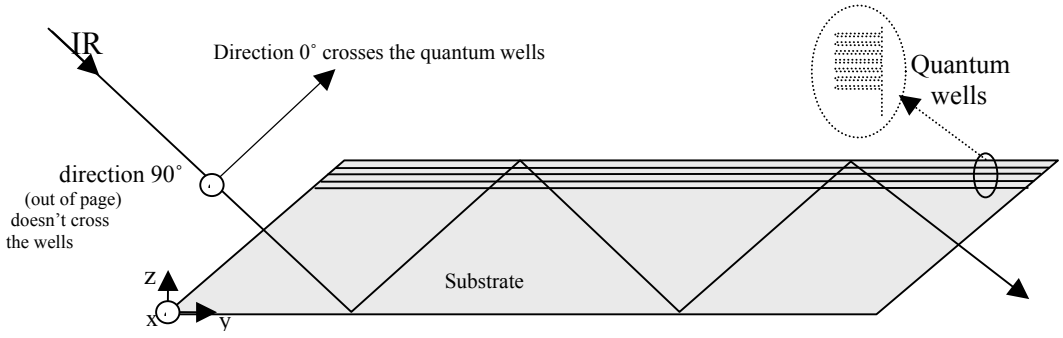

Figure 12. Wave-guide structure used for measurement of bound to continued inter-sub-band transition. The 0˚ and 90˚ show the direction of photon electric field relative to the angle on the polarizer used.

The quantum wells are formed along the growth z-direction. Absorption occurs only if the polarization of incident light has a component along the z direction (Levine 1993). This implies that the light incident along the normal (z direction) will not be detected. This is known as the polarization selection rule.

The FTIR spectrometer used in this thesis is the NEXUS 870 FT-IR system made by Thermo-Nicolet. The system incorporates a Windows-based Omnic software package as a build-in tool. It utilizes a rapid scanning interferometer, which is capable of better than 0.1 cm^{-1} resolution. It also converts the detected interferogram into a spectrum digitally.

3. Preparation of Wave-Guide

The infrared absorption measurements carried out at room temperature using a waveguide polish on the sample to enhance the absorption by multiple reflections and overcome the polarization selection rule. Parallel 45^{o} facets were lapped and polished at opposing ends of the sample to allow multi-pass transmissions during the FTIR spectroscopy measurements as illustrated in Figure 13. The waveguide-sample 0.5 mm thick and 4 mm long was placed in the sample compartment of the FTIR as illustrated in Figure 13.

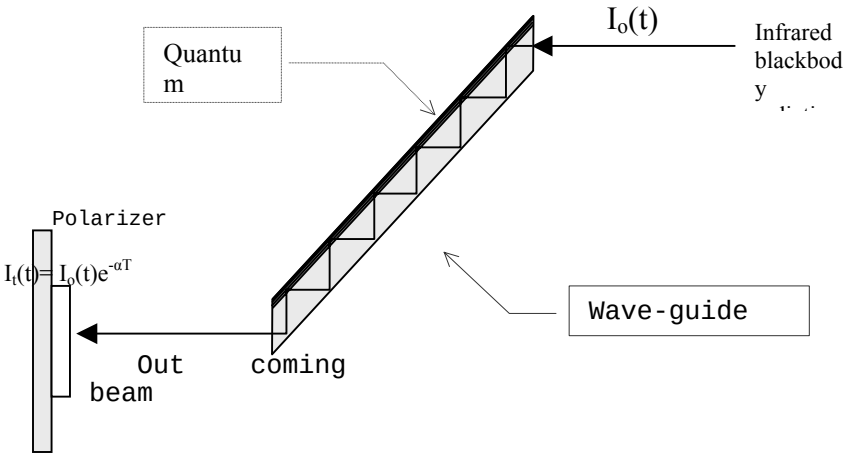

Figure 13. The schematic of the polished wave-guide.

Un-polarized infrared radiation entering at normal to one of the facets experiences multiple internal reflections from the boundaries of the sample. The outgoing beam passes through a polarizer before it is finally detected by the spectrometer. The absorption spectrum of the sample is collected after the substrate background spectrum has been

obtained to subtract the absorption due to the background and the substrate.

B. FTIR MEASUREMENTS

1. Infrared Absorption Spectra

The infrared absorption spectra measured for different polarization angles for the *mirror-like step* quantum well structure are shown in Figure 14.

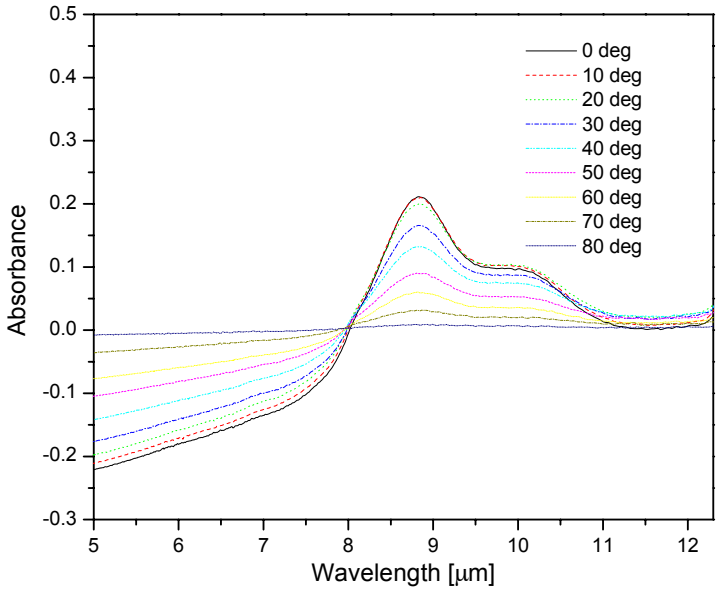

Figure 14. The absorption spectra, of the fabricated MQW structure at 300 K in different polarization angles.

The spectrometer measures the Absorbance which is defined as: Absorbance = -log(Transmittance). The Transmittance is the ratio of transmitted power (I_t) to the incident power (I_o). The absorption coefficient of the structure is given by

$$\alpha = -\frac{1}{w}\ln\left(\frac{I_t}{I_o}\right)$$

Where w, is the total thickness of the absorbing region, including multiple passes through the wave-guide.

2. Base Line Corrected Infrared Absorption Spectra

All of the absorption spectra found to be “tilted” in Figure 14; are due to the free carrier absorption in the quantum wells in addition to the inter-sub-band transitions. The software package of the FTIR spectrometer provides the automatic baseline correction tool, although the base line correction can be accomplished manually by starting and ending the points of the line segment. The baseline corrected infrared absorption spectra for different polarization angles are illustrated in Figure 15.

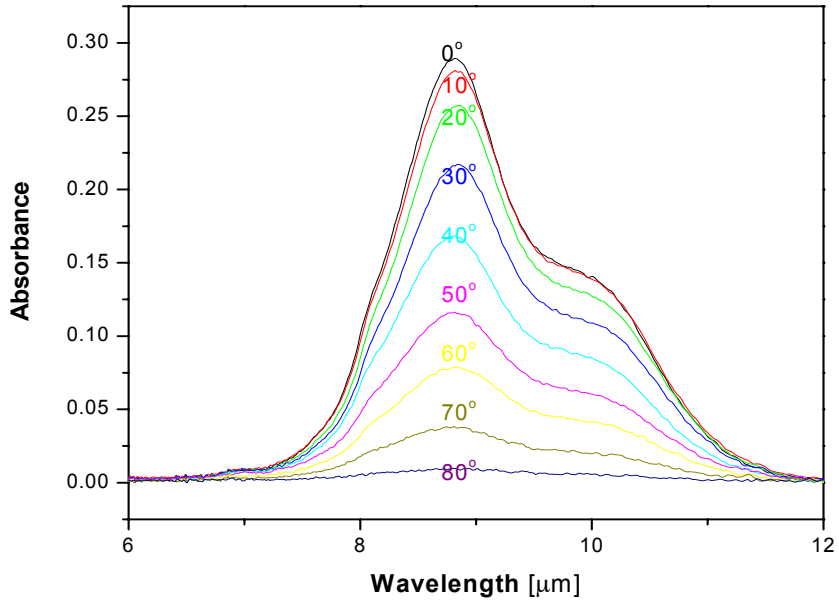

Figure 15. The baseline corrected absorption spectra of the fabricated MQW structure at 300 K in different polarization angles.

From the FTIR spectra two absorption peaks are found at **8.8** μm (**1130** cm^{-1}), and at **10.0** μm (**970** cm^{-1}) due to the two mirror-like step wells.

3. Lorentzian Fit

The absorption spectra shown in Figure 15 consist of two peaks due to the different energy levels separations of the two-step wells. We can separate the two absorption peaks by fitting two Lorentzian curves, one for each absorption peak. The two Lorentzian fits are shown in Figure 16 and they give a better understanding of the absorption spectra for each step well of the grown MQW structure.

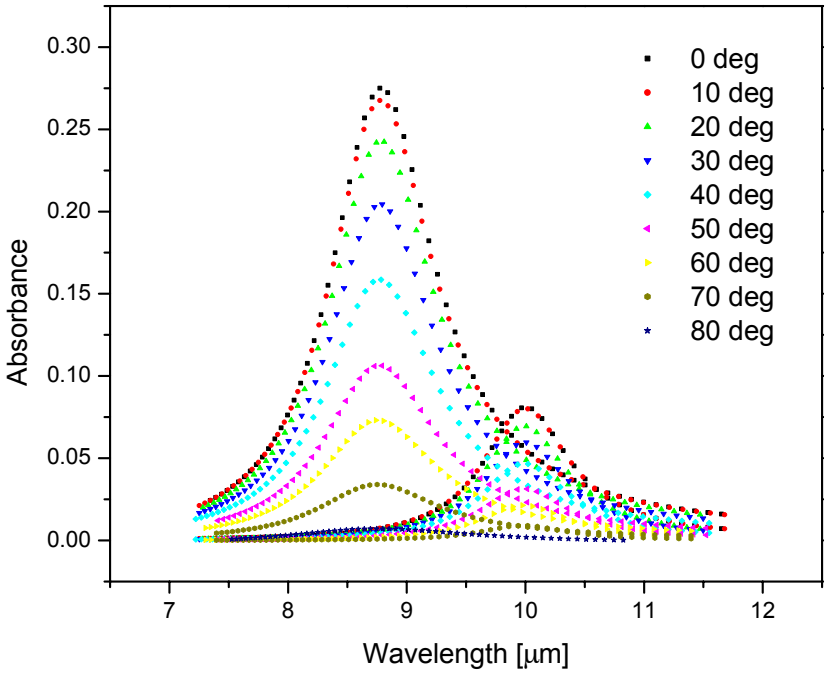

Figure 16. Lorentzian fit of the MQW absorption spectra. Each fit corresponds to the one of the two different step wells at different polarizations.

C. ABSORPTION ANALYSIS AND SIMULATION

1. Absorption Coefficient and Oscillator Strength

The absorption coefficient α can be found from the FTIR absorption spectra. The peak of the absorbance for transverse magnetic (TM) mode incident light is 0.30. Using the definition of the absorbance we can get the absorption coefficient α_p, as follow:

$$\alpha_p = -\frac{1}{w}\ln\left(10^{-\text{Absorbance}}\right)$$

The width w can be calculated considering the path of the infrared beam inside the wave-guide. The number of reflections through the wave-guide is 6, which is obtained by taking the ratio length/thickness of the wave-guide. The width of one period of MQW is 370 Å for each step well, and the number of periods is 20, so the total absorption length w is $4.44\,\mu m$. Using the measured peak absorbance for the two peaks, the estimated absorption coefficients are $\alpha_{p1}=1550 cm^{-1}$ and $\alpha_{p2}=440 cm^{-1}$ respectively.

The oscillator strength (f) of the transitions can be estimated using (Zhou 2001):

$$\alpha_p = \frac{\rho_s N e^2 \hbar f}{L\sqrt{\varepsilon_r}\,\varepsilon_o m^* c\Gamma}\frac{\sin^2\theta}{\cos\theta}$$

Where $\rho_{s1}=4\times10^9/cm^2$ and $\rho_{s2}=3\times10^9/cm^2$ are the two dimensional density of electrons in the two step wells, N is the total number of quantum wells that the IR beam crosses, e is the electron charge, $\hbar$ is the reduced Plank's constant, L=370 Å

is the period of the MQW, Γ=0.018 eV (Γ=0.012 eV) is the full width at half maximum of the first and second peak, θ=45^{o} is the incident angle inside the wave-guide, ε_r=12.4 is the relative dielectric constant of GaAs, m*=0.067m_o is the electron effective mass where m_o is the electron mass, and c is the velocity of light in vacuum. Using $\alpha_{p1}=1550cm^{-1}$ and $\alpha_{p2}=440cm^{-1}$, from above we obtain oscillator strengths for the two peaks as:

$$f_{(\Gamma=0.018\ eV)}=0.60,\quad f_{(\Gamma=0.012\ eV)}=0.40.$$

2. Polarization Dependence

One of the characteristics of inter-sub-band transitions is the cosine square polarization dependence of the strength of absorption peak (Levine 1993). The measured peak absorption plotted against the squared cosine of the polarization angle is shown in Figure 17, and found to be in good agreement with the cosine theoretical prediction.

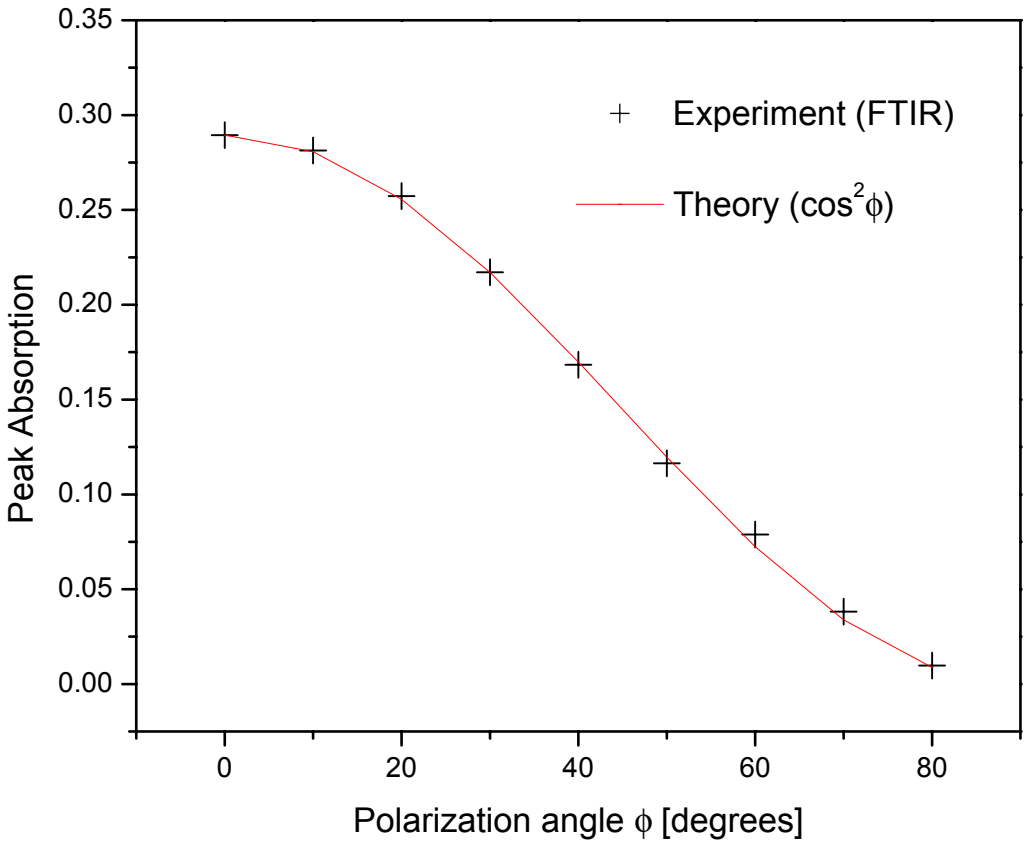

Figure 17. Plot of peak absorbance as a function of polarization angle.

3. Absorption Simulation

In the fabricated MQW structure, the step wells are isolated from each other due to the wide potential barriers between them. As a result the absorption in the wells can be approximated to that of a single well (Levine 1992). The transfer matrix method (TMM) is the most versatile technique in obtaining the energy states, the transmission coefficient and the corresponding wave functions of an arbitrary potential profile (Lantz 2002). Using the Schrödinger equation, the boundary and the normalization conditions, we can find the energy levels, the absorption coefficient and the oscillator strength of the structure with the aid of a computer program (Lantz 2002). The energy levels, the absorption peak and the oscillator strength of the first step quantum well of the mirror-like structure (see Figure 7) are illustrated in Figure 18.

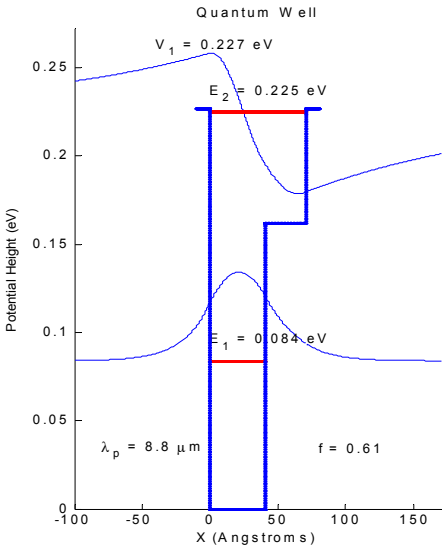

Figure 18. The Energy levels, the absorption peak and the oscillator strength found for the first step quantum well of the mirror-like structure of the fabricated MQW structure.

The energy levels, the absorption peak, and the oscillator strength, of the second step quantum well of the mirror-like structure are illustrated in Figure 19.

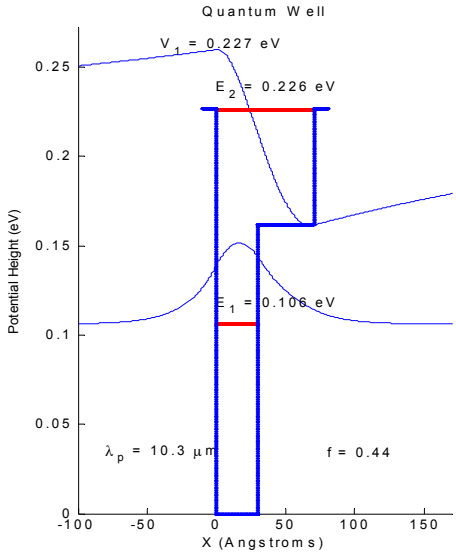

Figure 19. The Energy levels, the absorption peak and the oscillator strength found for the second step quantum well of the mirror-like structure.

The simulation gives theoretical values of the absorption peak position, and oscillator strength which are in good agreement with the experimentally values found with FTIR spectroscopy as shown in table 1.

COMPARING		**EXPERIMENT** (FTIR)	**SIMULATION** (TMM)
First QW	Absorption peak λ_p [μm]	8.8	8.8
	Oscillator strength f	0.60	0.61
Second QW	Absorption peak λ_p [μm]	10.0	10.3
	Oscillator strength f	0.40	0.44

Table 1 : Comparison of experimental and simulate results.

In the following chapter, we will describe the detector fabrication and I-V characterization.

THIS PAGE INTENTIONALLY LEFT BLANK

III. CURRENT VS VOLTAGE (I-V) CHARACTERISTICS

A. INTRODUCTION

1. Device Fabrication

In order to characterize the TB-QWIP design, the epitaxial wafer processed, by professor Mei Ting's group in Nanyang Technological University (NTU) in Singapore, using standard photolithography techniques. The processed wafer contains detectors with dimensions ranging from 80x80 to 300x300 μm^2. The latter devices were used in this thesis. A set of detectors assembled in the Sensor Research Laboratory at NPS by cutting the processed wafer, and polishing a 45^o facet to couple to the IR, and mounted on a ceramic chip carrier. The detectors are wire bonded to the contact pads of the chip carrier using a Kulicke & Soffa (Model 4524A) wire bonder. The details of the assembly process are described in Touse (2003). The test chip used in this thesis contained seven operating test detectors assembled by the author, and is illustrated in Figure 20. The test detectors named with capital letters from A through G from left to right as shown in Figure 20.

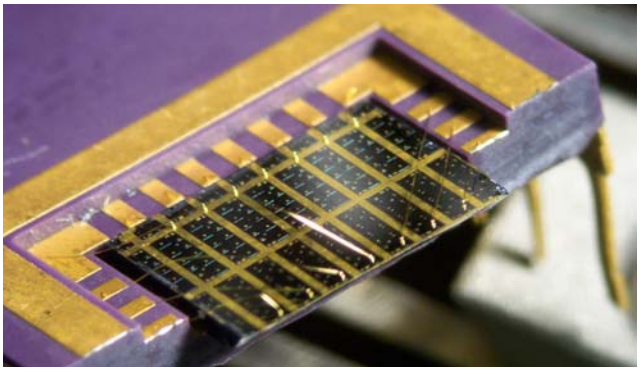

A B C D E F G

Figure 20. The test detector with seven wire-bonded detectors named A through G.

B. I-V MEASUREMENTS

1. Current Vs Voltage Detector Parameter

The current versus applied voltage is an important characteristic that can determine the optimum operating point of a detector. The I-V curves are also used to determine the amount of leakage current at various temperatures, which can provide information on the barrier height (Hickey 2002) from the ground state of the quantum well. A schematic diagram showing the collection of excited charge carriers (due to both the thermionic emission and background IR) from the QW with an applied bias is shown in Figure 21.

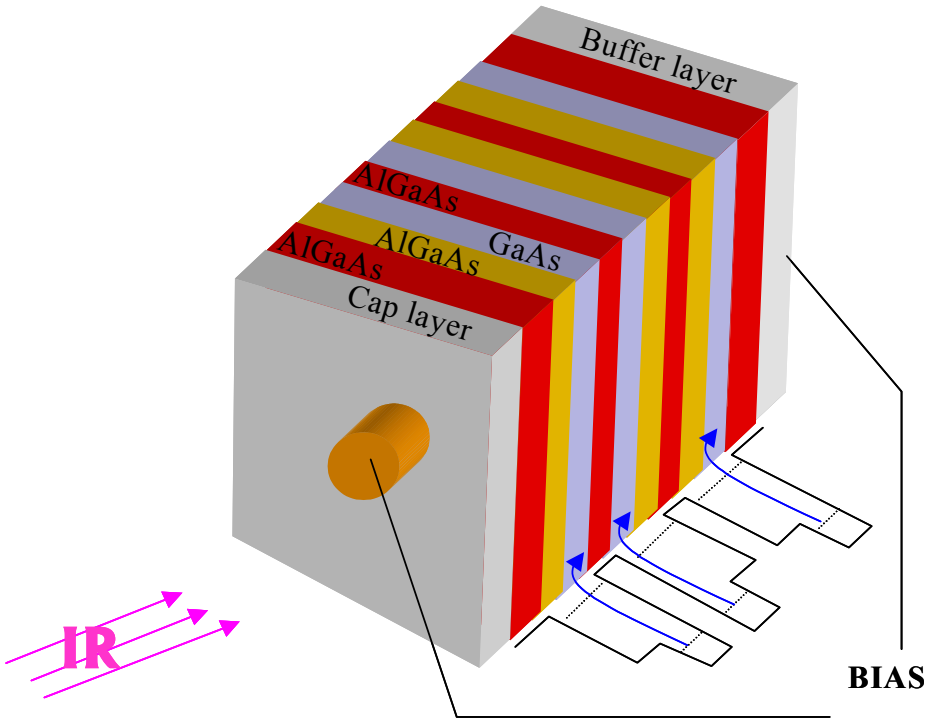

Figure 21. Simplified diagram showing the collection of excited charge carriers from the QW with an applied bias.

2. Dark Current

In order to measure the dark current, the chip was covered using an aluminum foil to form a cold shield to eliminate the photocurrent due to background thermal radiation. Measured *I-V* characteristics of the test detector (named D) between 10 and 150 K in steps of 10 K are shown in Figure 22. The *I-V* characteristics are relatively insensitive to temperature below 40 K, while the high temperature regime (>50K) shows strong temperature dependence. The dramatic reduction of the dark current at low temperatures is largely due to the decrease of thermionic emission. The positive bias refers to positive potential on the cap layer contact.

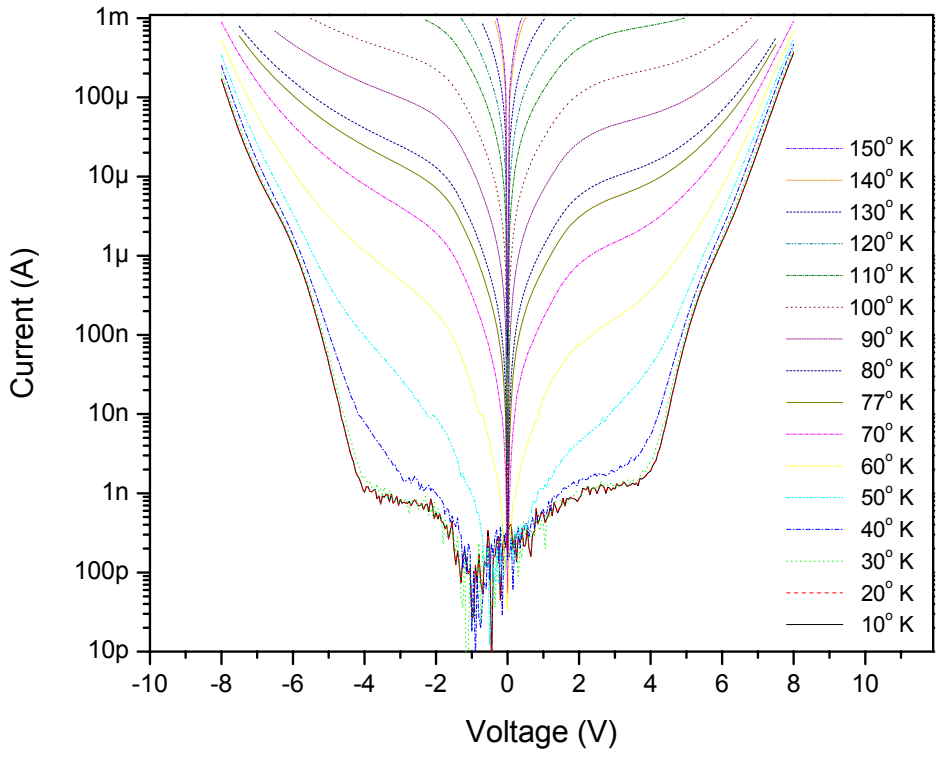

Figure 22. The dark condition *I-V* characteristics.

3. Background Limited Current

In order to find the background limited current due to background thermal radiation, the test detector was uncovered and the *I-V* characteristics measured between 10 and 150 K in steps of 10 K are shown in Figure 23.

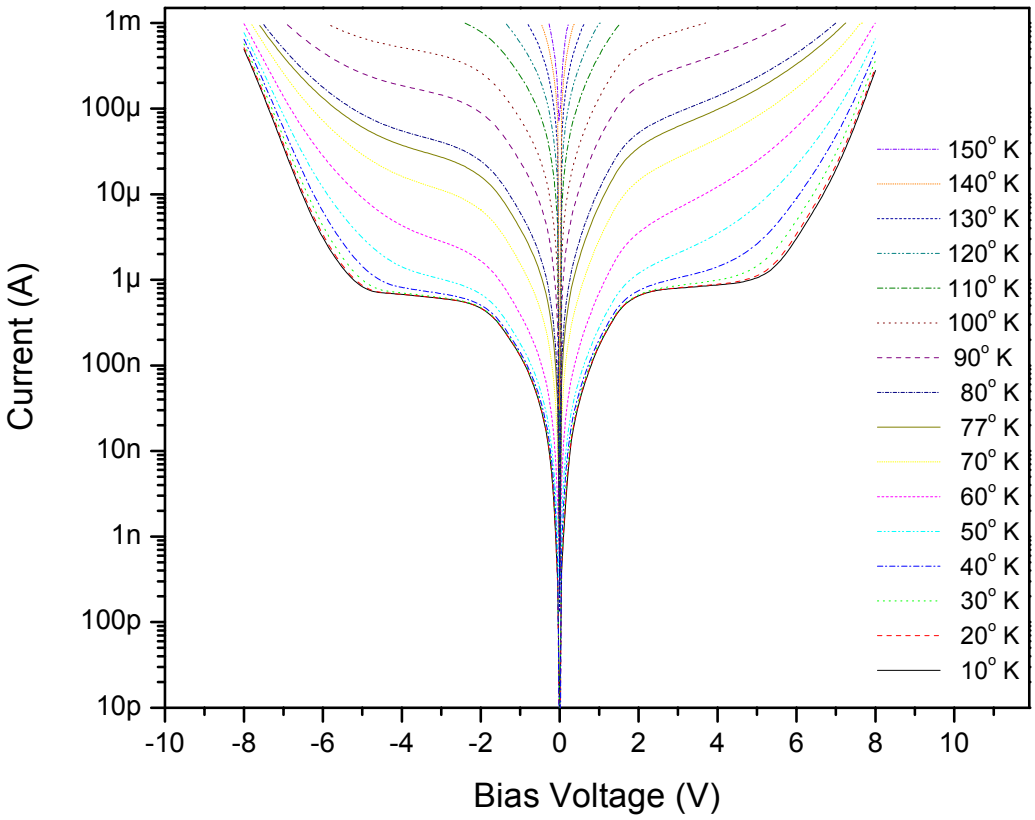

Figure 23. The *I-V* characteristics with the test detector exposed to 180° field of view background radiation.

The substantial increase of the current at low temperature (10-50° K) is mainly due to the photocurrent generated by the background IR radiation.

C. I-V ANALYSIS

1. Temperature Under Background Limited Condition

In order to determine the background-limited operating temperature (T_{BLIB}), the background generated current at 10^{o} K is plotted along with dark-current at different temperatures as depicted in Figure 24.

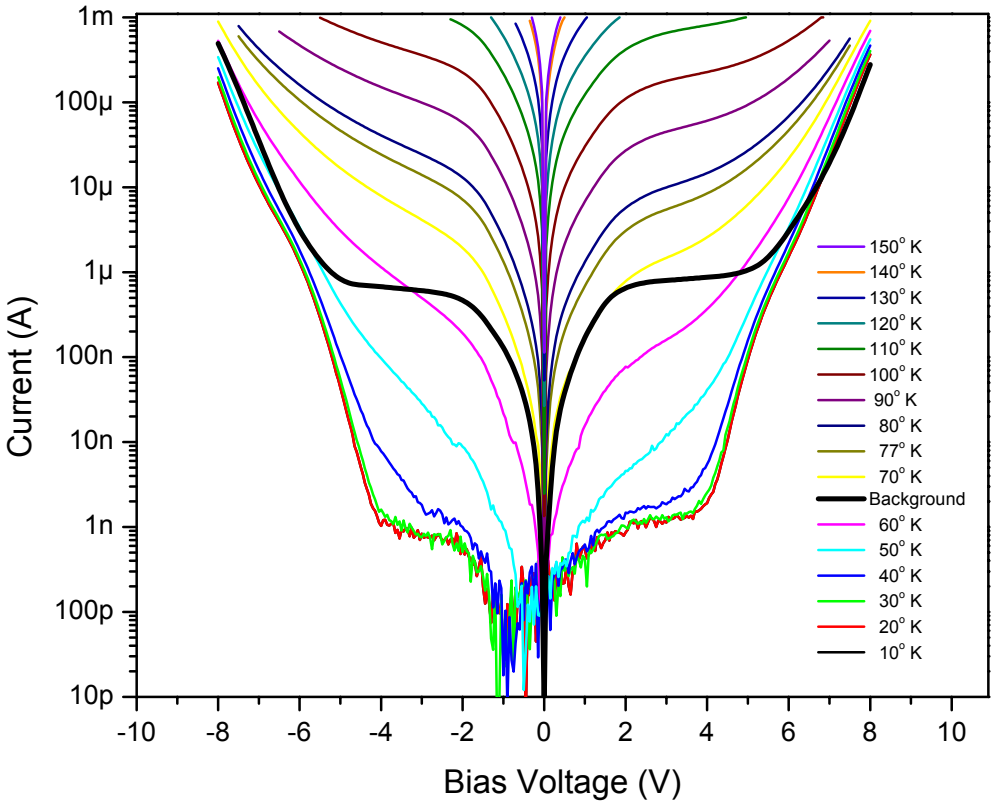

Figure 24. The *I-V* characteristics of the test detector.

It can be clearly seen from Figure 24 that the background-limited performance of the test detector occurs between 50-60K.

2. Operating Temperature

The I-V characteristics for temperatures below 55 K with background radiation are relatively insensitive to temperature. The current for bias voltages greater than 4 volts is mainly due to tunneling. This behavior is illustrated in Figure 26, which shows a small, steady tunneling current at voltages less than 4 volts. At voltages above 5 volts, however, the current increases rapidly as it becomes easier to tunnel through a reduced barrier thickness.

Since a room temperature background causes a photocurrent greater than the dark current at 55 K, cooling the device lower than 55 K will not lower the noise generated by the detector and would be a wasted effort in an operational setting. The background-limited performance of the device when biased with –4 V, occurs at approximately 55 K where the dark current is nearly the same as the background generated photocurrent. Though, when the device biased with +4 V the background-limited performance occurs at approximately 60 K. This is because the tunneling carriers are facing a wider step barrier when the QW structure is forward biased.

IV. PHOTOCURRENT SPECTROSCOPY

A. INTRODUCTION

1. Photo Response

In order to study the performance of the TB-QWIP, it is necessary to measure the photo response of the detector at different bias voltages. This can be conveniently achieved by photocurrent spectroscopy. In the following, we will first describe the system used in this measurement.

2. Equipment and Set Up

The photocurrent spectroscopy is carried out using a designed computer controlled characterization system, initially developed by Herdlick (2002), and software modified by Touse (2003). In the characterization system a Quartz-Tungsten-Halogen source is used for the visible region and to align the optical beam. A dedicated IR element operated at 1150 K provided gray-body radiation to cover the near to mid infrared wavelengths. A monochromator in conjunction with a six-position filter wheel provided precise control of energy incident on the photo detectors. The system includes two lock-in amplifiers that are frequency referenced to an optical chopper, an electronics breadboard for circuit manipulation, and a power supply for biasing the device. As described in Herdlick (2002), the detector response was compared to a flat-response reference detector to account for variations in power emitted by the source and absorbed along the optical path. The reference detector used has a constant responsivity of 1000 V/W with an area of 5 mm x 5 mm. A front-coated silver mirror was

used for switching the beam between the test and reference detectors. The photocurrent spectroscopy setup with the detector inside the refrigerator is illustrated in Figure 25.

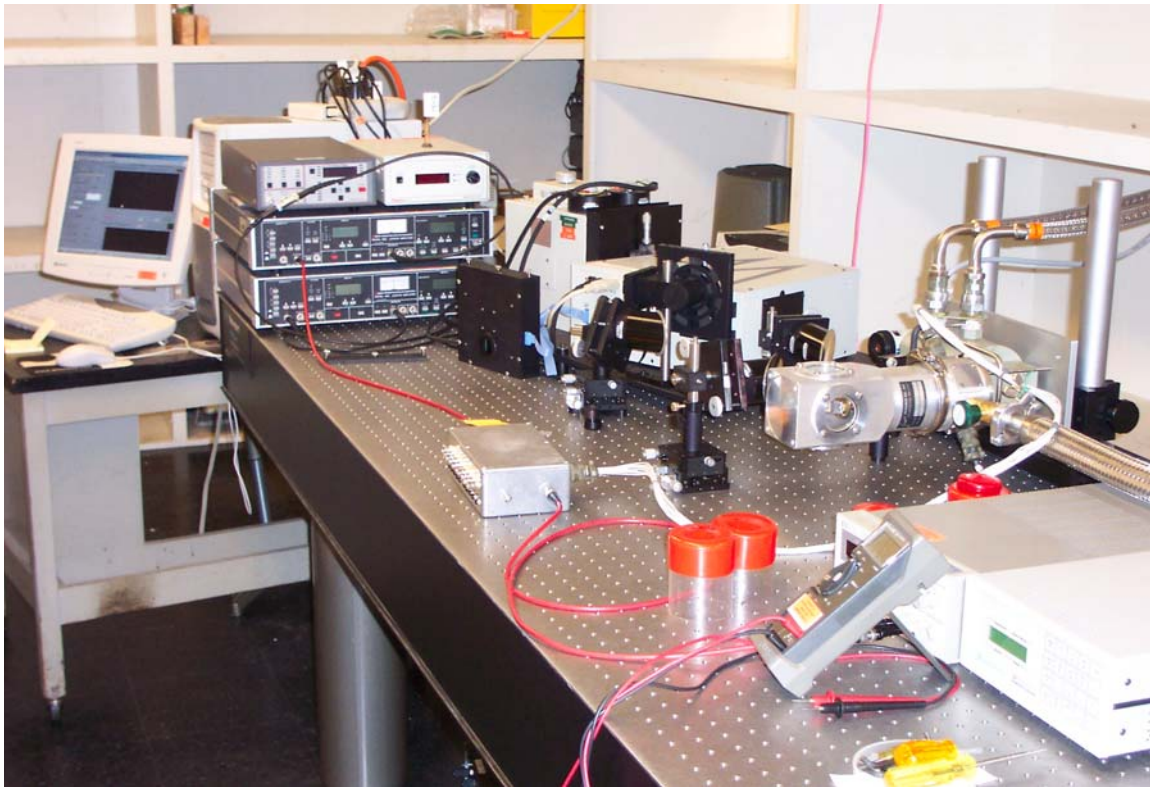

Figure 25. The photocurrent spectroscopy setup.

3. Calculation of Responsivity and D*

The responsivity, $\Re$ of the test detector, is defined as $\Re_D = \frac{I_D}{\phi_D}$, where ϕ_D is the flux or power incident on the device, and I_D is the photocurrent. The flux incident on the

reference detector can be defined as $\phi_R = \frac{V_R}{\Re_R}$, where V_R and $\Re_R$ are the photo voltage produced by the reference detector and its responsivity, respectively. The intensity on both the reference detector and the test detector are considered the same since the path lengths and optics are nearly the same for both detectors. Therefore, the flux incident on the test detector, ϕ_D, is proportional to the ratio of illuminated areas of the test and the reference detectors. The power incident on the test detector is reduced by a factor of $1/\sqrt{2}$ due to the 45° angle between the detector area and the incident beam. In addition, the light incident on the device had to be corrected to take into account the reflections at the window and the 45° facet. The transmission coefficient of Zinc-Selenide (T_{ZnSe}) is 0.6 (Touse 2003). The transmission coefficient at the air-GaAs interface is T_{GaAs}=0.68 (Kasap, 2002). Including all the above mention factors, the power incident on the detector can be written as $\phi_D = \phi_R \frac{A_D}{A_R} = \frac{V_R}{\Re_R}\frac{A_D}{A_R}$, where A_D=(0.3mm)^2 and A_R=5mm·2mm are the area of the test and reference detectors, respectively. Finally the responsivity of the test detector is given by

$$\Re_D = \frac{I_D}{\phi_D} = \frac{I_D}{V_R}\left(\Re_R \frac{A_R}{A_D}\frac{\sqrt{2}}{T_{GaAs}T_{ZnSe}}\right) = \frac{I_D[nA]}{V_R[mV]}\left[0.385\frac{V}{W}\right].$$

This formula gives the responsivity of the test detector in A/W when the photocurrent of the test detector is measured

in nano-amperes and the photo voltage of the reference detector is measured in mili-volts.

The circuit shown in Figure 26 was used to measure the current through the test detector, using the lock-in amplifier connected to the test detector operating in the ammeter mode. The lock-in amplifier attached to the reference detector is operated in the voltage mode since the reference detector provides a voltage output.

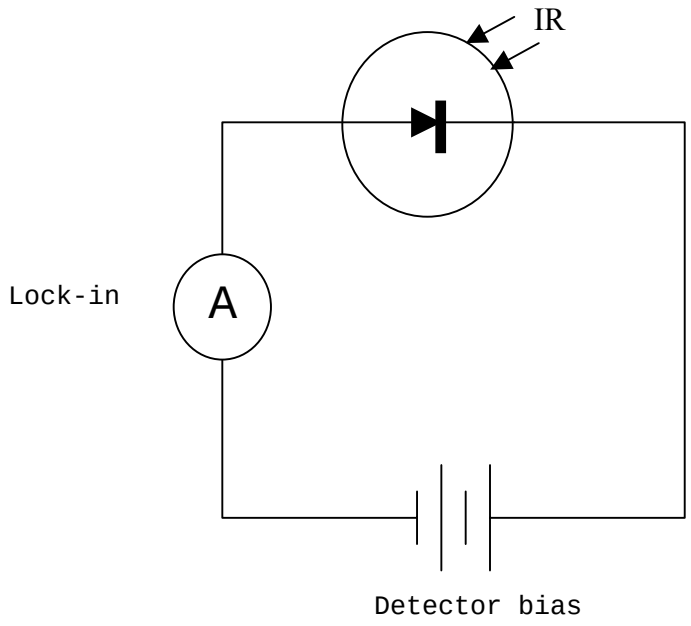

Figure 26. Circuit used to measure the photocurrent from the test detector.

B. PHOTOCURRENT MEASUREMENTS

1. Filters

The photocurrent (I_D) measurements were carried out for wavelengths ranging from 5μm to 12μm to prove the relative broad spectral response of the detector. It was necessary to use two different filters during the measurement since the filter cutoff wavelengths happened to lie at the bandwidth of interest. The photocurrent, I_D, as a function of wavelength corresponds to the two filters used shown in Figure 27.

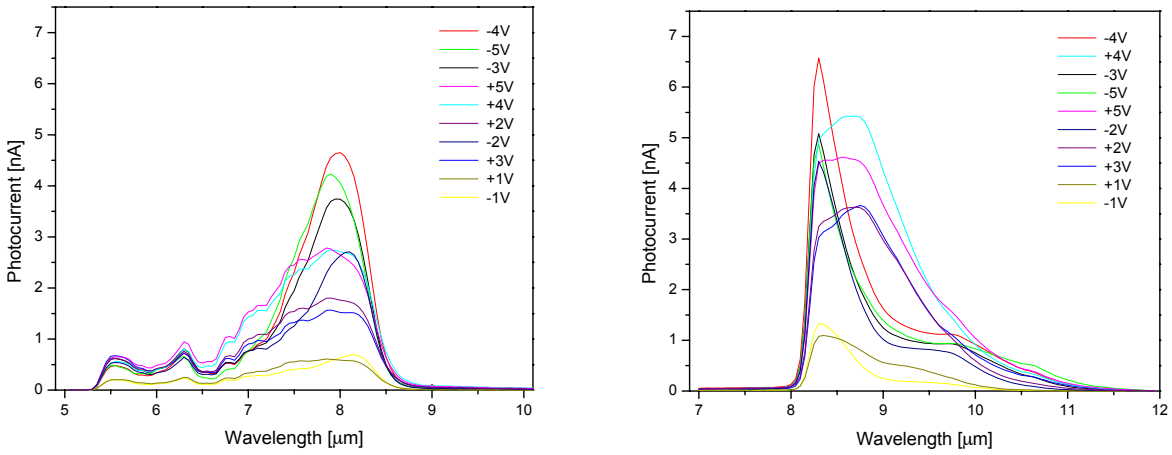

Figure 27. The photocurrent of the test detector measured using the two filters at a set of bias voltages. The measurement was carried out at 10°K.

The same measurement was repeated for the reference detector to estimate the intensity of the beam as a function of wavelength and the results are shown in Figure 28.

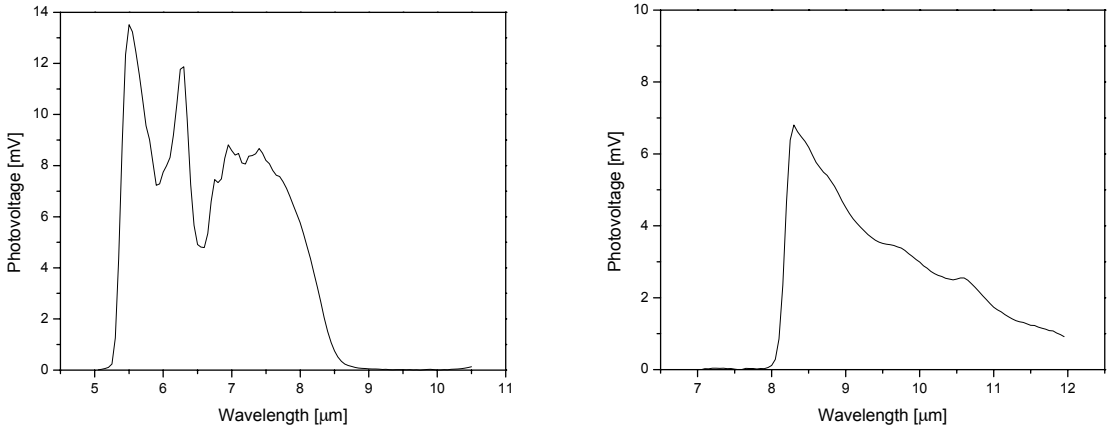

Figure 28. The measured signal of the reference detector as a function of wavelength.

The photocurrent and the photo-voltage measurements are divided to give the $\frac{I_D[nA]}{V_R[mV]}$ term for the estimation of the responsivity. After the division the results were multiplied with the constant factor $0.385\frac{V}{W}$, which was derived previously in the calculation of the responsivity.

2. Responsivity

The responsivity of the test detector as a function of wavelength for a set of forward bias voltages is shown in Figures 29 and 30, respectively. Forward bias refers to positive potential on the cap layer contact.

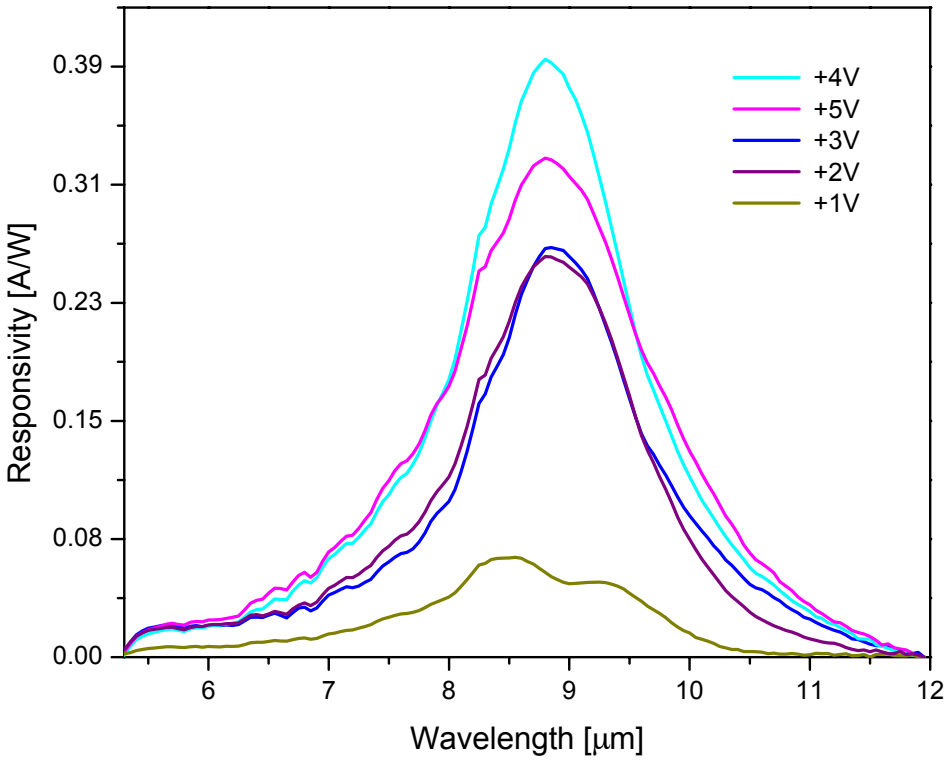

Figure 29. The responsivity of the TB-QWIP detector as a function of wavelength for a set of forward bias voltages.

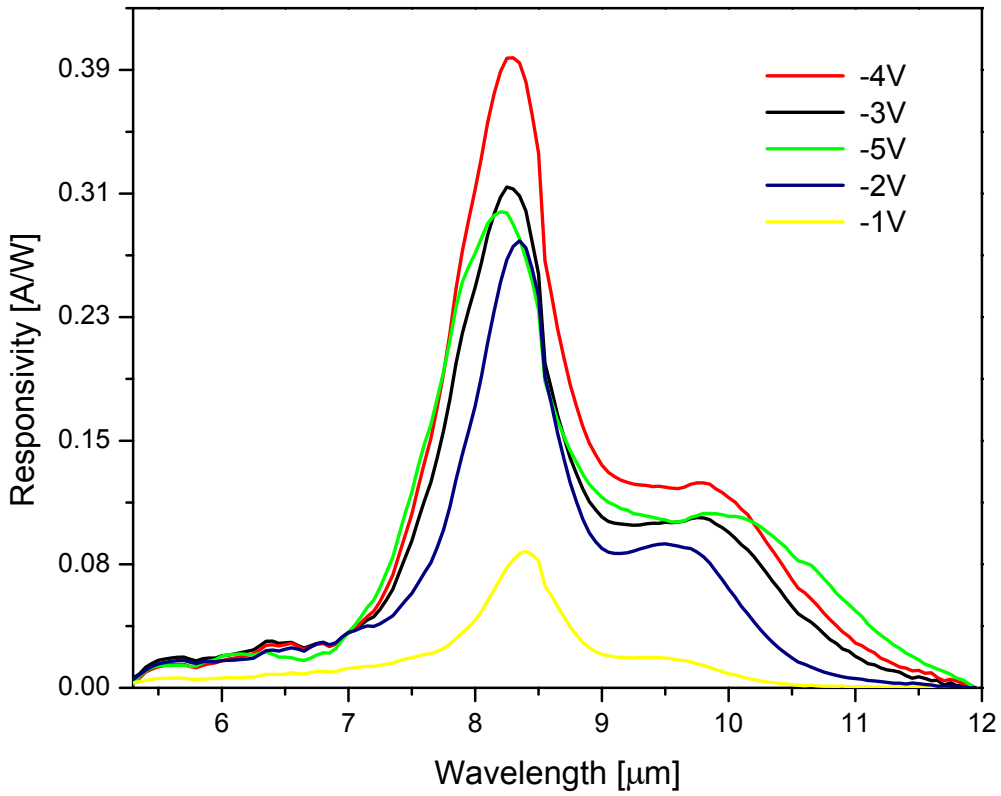

Figure 30. The responsivity of the TB-QWIP detector with reverse bias, and its reverse bias dependence.

The maximum value of the responsivity occurs at 4 V for either polarity of the bias. The measured maximum value of the responsivity is 0.4 A/W at 8.2μm wavelength for positive bias and at 8.8μm wavelength for negative bias.

3. Detectivity D^* and Quantum Efficiency

The Noise Equivalent Power (NEP) is given as (Dereniak and Boreman, 1996, p.203) $NEP = \frac{I_n}{\Re_D}$, where I_n is the noise current whose major contributions are noise from thermal motion (Johnson noise), generation and recombination of electrons (G-R noise), and noise from electrons traversing a potential barrier (shot noise). The detectivity D* is then defined as

$$D^* = \frac{\sqrt{A_D \cdot \Delta f}}{NEP} = \frac{\Re_D \sqrt{A_D \cdot \Delta f}}{I_n}.$$

Since the test detector is a photoconductor the main contribution to the noise comes from the generation and recombination of carriers. The corresponding noise current is given by: $I_n = \sqrt{4eGI_D \Delta f}$, where G is the optical gain and is considered to be unity in this case, I_D is the total current through the device, and Δf is the frequency bandwidth which is usually taken to be 1 Hz (Levine, 1993). This gives the final detectivity equation of

$$D^* = \Re_D \sqrt{\frac{A_D}{4eI_D}} \quad \text{cm}\sqrt{\text{Hz}}/\text{W}$$

The detector figure-of-merit is usually described by the detectivity under the background limited performance (BLIP) condition where the total current through the detector is due to photo-generation from the background IR. We have measured this current and found to be about 1μm at 4 V bias. The corresponding D^* is 3.5x10^{11} $\text{cm}\sqrt{\text{Hz}}/W$, which is comparable with reported QWIP detectors (Levine 1993).

Another useful detector parameter is the quantum efficiency, which is calculated from $\eta = \frac{I_D/e}{\phi_D/h\nu}$, and the maximum value the detector is found to be 6%.

C. ANALYSIS OF TUNABILITY

1. Bias Dependence of Peak Position

In order to analyze the photocurrent data and characterize the test detector, the data of Figures 31 were Lorentzian fitted to separate the response from the two quantum wells. The Lorentzian fitted responsivity data of the test detector are shown in Figure 31, and have two peaks due to the different energy separation in the first and the second step wells. The two absorption peaks were separated for all the bias voltages by fitting two Lorentzian fits for each responsivity curve. The Lorentzian fits shown in Figure 31 are normalized, and they give a better representation of the responsivity position peak shift as a function of forward and reverse bias.

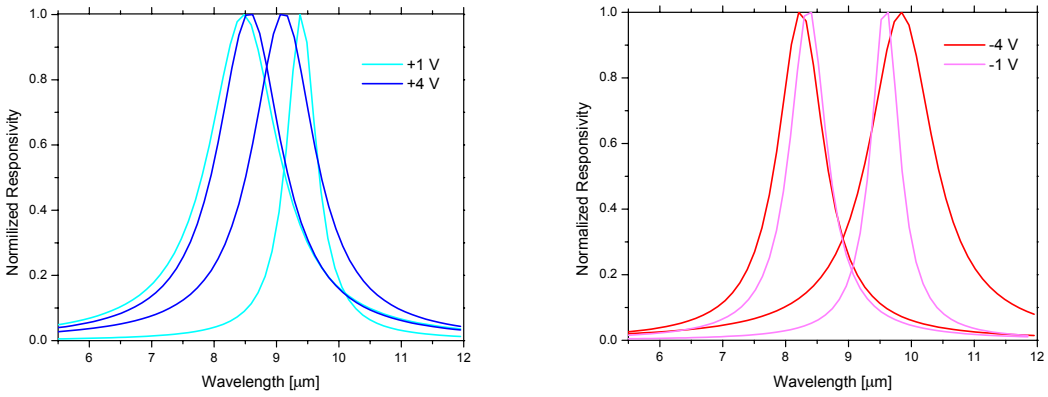

Figure 31. The normalized responsivity of the TB-QWIP for deferent biases.

The linear Stark effect associated with step quantum wells is responsible for the peak shift towards longer wavelengths under forward bias (Mii, *et al.*, 1990). The peak positions of the TB-QWIP are coming closer to each

other with positive bias and moving away from each other with negative bias. This is in agreement with the initial TB-QWIP theoretical design, and indicates the possibility of controlling the detector bandwidth using external bias. Figure 32 shows the responsivity position peak shift as a function of bias. The peak shift results in a wider bandwidth.

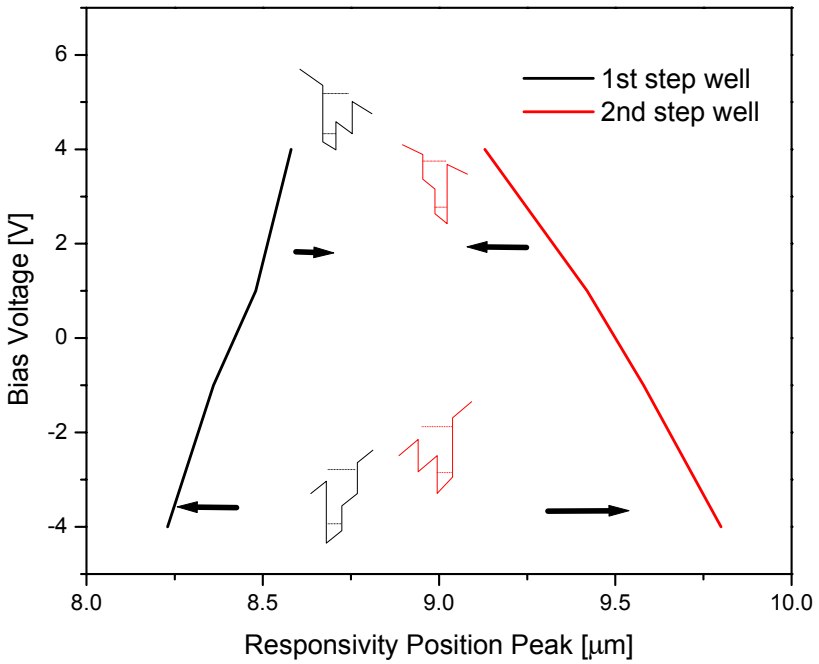

Figure 32. The position peak shift of responsivity of the TB-QWIP as a function of bias.

2. Bandwidth Tunability

The bandwidth tunability of the test detector is shown in Figure 33, which is taken to be the half width at full maximum of the normalized responsivity as a function of bias.

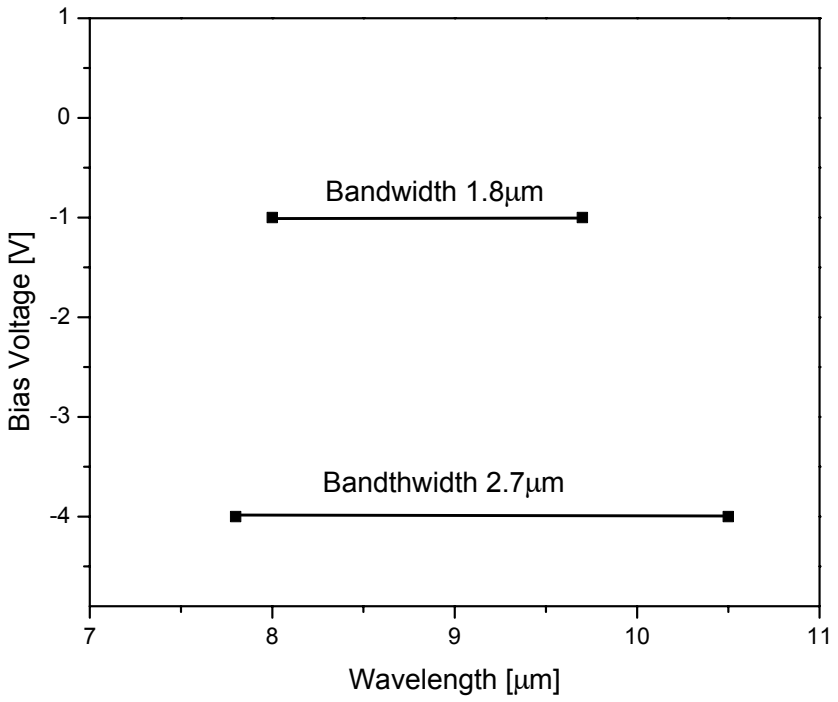

Figure 33. The bandwidth tunability of the test detector.

The tunability of the detector is:

$$Tunability = \frac{\Delta(Bandwidth)}{Bandwidth} = \frac{0.9}{1.8} = 0.5 \quad \text{or} \quad \boxed{Tunability = 50\%}$$

3. Further Research

A useful conclusion from the analysis of the photo-response of the test detector can be extracted from Figure 38 for the second step quantum well, which is revealing a tunable behavior of close to 100%. That is because the wider step-width of the second step well results the larger the stark shift effect, and this is in agreement with the separation of the center of the wave functions as shown in Figures 18, and 19. Thus the second step well design is more suitable for the TB-QWIP. Further research is required to optimize the epitaxial structure by using the second QW, which holds promise for 100% tunability or more.

V. CONCLUSION

In this thesis a tunable bandwidth quantum well photo detector (TB-QWIP) was fabricated, and experimentally characterized.

The characterization of the TB-QWIP was based on absorption measurements with Fourier Transform Infra Red (FTIR) spectroscopy, current versus applied voltage analysis with a semiconductor analyzer, and photocurrent spectroscopy using a computer control characterization system. The IR absorption peaks at room temperature, were found to be at 8.8 μm and 10.0 μm with bandwidth of about 1.8 μm in agreement with simulation. The Dark current of the test detector was found to be 1.0 x 10^{-9}A and a background photocurrent found to be 700 x 10^{-9} A at -4 V bias at 10 K. The background-limited performance of the detector was found to occur at about 60 K. The maximum responsivity was 0.4 A/W at 8.2 μm. The maximum normalized detectivity under background limited conditions D^*_{BLIP}, was calculated to be $3.5 \times 10^{11} \mathrm{cm}\sqrt{\mathrm{Hz}}/W$. The bandwidth of the detector can be tuned with bias from 1.8 μm to 2.7 μm, which corresponds to a bandwidth tunability of about 50%.

Further research is required to optimize the sample structure by using the second step QW of this design, which holds promise for 100% tunability or more.

THIS PAGE INTENTIONALLY LEFT BLANK

APPENDIX A

Fabricated sample profile for a single period

Profile	Mole %	Thickness (A)	Doping (cm^{-3})
GaAs		5000	10^{18}
AlGaAs	28	300	
GaAs		30	10^{18}
AlGaAs	20	40	
AlGaAs	28	300	
AlGaAs	20	30	
GaAs		40	10^{18}
AlGaAs	28	300	
GaAs		8000	10^{18}
GaAs substrate		635 μm	

THIS PAGE INTENTIONALLY LEFT BLANK

LIST OF REFERENCES

Bandara S. V., S. D. Gunapala, J. K. Liu, E. M. Luong, J. M. Mumolo, W. Hong, D. K. Sencupta and M. J. McKelvey *"10-16 μm Broadband quantum well infrared photo detector"* Center for space Microelectronics Technology, Jet Propulsion Laboratory (1997)

Bandara S. V., S. D. Gunapala, D. Z. Y. Ting, S. B. Rafol, and J. K. Liu, *"GaAs/AlGaAs multi-quantum-well based far infrared detectors for astronomy application"* Jet Propulsion Laboratory California Institute of Technology (2001)

Capasso Federico, *"Band-gap engineering and interface engineering: novel super lattice structures and tunable band discontinuities"*, AIP Conference Proceedings Vol 138(1) pp. 170-183. April 20, 1986

Choi K. K. *et al "Infrared photoelectron tunneling spectroscopy of strongly coupled quantum wells"*, Phys. Rev. B 39, 8029 (1989)

Coon, D.D. and R.P .a. Karunasiri, "*New mode of IR detection using quantum wells*", Appl. Phys. Lett., 45, pp.649-651, 1984.

Coon, D.D. and R.P .G. Karunasiri and L.Z. Liu, "*Narrow band infrared detection in multi-quantum well structures*", Appl. Phys. Lett., 47, pp.289-291 , 1985.

Ferry, David K.: *Gallium Arsenide Technology*. Indianapolis, Indiana, Howard W. Sams & Co., Inc., 1985, pp. 21-46.

Griffiths P. R. and J.A. de Haseth, *"Fourier Transform Infrared Specctrosopy"*,John Wiley & Sons, New York (1986).

Gunapala S. D. and S. V. Bandara, *"Quantum Well Infrared (QWIP) Focal Plane Arrays"*, Semiconductors and Semimetals series, Vol. 62, (1999)

Hasnain, G., B.f. Levine, D.L. Sivco and A.Y. Cho, "*Midinfrared detectors in the 3-5 μm band using bound to continuum state absorption in InGaAs/InAlAs multi quantum*

well structures", Appl. Phys. Lett., 56, pp. 770- 772, 1989.

Herdlick, Brian E., *Computer-Controlled Photo-detector Characterization System (Design and Construction),* Master's Thesis, Naval Postgraduate School, Monterey, California, December 2002.

Hickey, Thomas R., *Temperature Dependence of Dark Current in Quantum Well Infrared Detectors,* Master's Thesis, Naval Postgraduate School, Monterey, California, June 2002.

Karunasiri, R.P.G., Y.J. Mii and K.L. Wang, "Tunable infrared modulator and switch using Stark shift in step quantum wells", IEEE Electron. Dev. Lett., 11, pp. 227-229, 1990.

Konukbay, Atakan, *Design of a Voltage Tunable broadband Quantum Well Infrared Photo-detector*, Master's Thesis, Naval Postgraduate School, Monterey, California, June 2002.

Lantz, Kevin R., *Two-Color Photo-detector Using An Asymmetric Quantum Well Structure,* Master's Thesis, Naval Postgraduate School, Monterey, California, June 2002.

Levine, B.F. K.K. Choi, C.G. Bethea, J. Walker and R.J. Malik, "New 10 μm infrared detector using inter-sub-band absorption in resonant tunneling GaAIAs superlattices", Appl. Physics Lett., 50, pp. 1092-1094,1987.

Levine B. F., C. G. Bethea, V. O. Shen, and R. J. Malik "Tunable long-wavelength detectors using graded barrier quantum wells grown by electron beam source molecular beam epitaxy" Appl. Phys. Lett. 57(4) 383 (23 July 1990)

Levine, B.F., A. Zussman, S.D. Gunapala, M.T. Asom, J.M. Kuo and W.S. Hobson, "Photo-excited escape probability, optical gain, and noise in quantum well infrared photo-detectors", Jour. Appl. Phy., 72, pp. 4429-4443, 1991.

Levine B.F., Zussman a., "Photo-excited escape probability, optical gain, and noise in QWIP", J. of Applied Physics 72(9), November 1, (1992)

Levine B. F. "Quantum-well infrared photo-detectors", Jour. Appl. Phys., 74, pp. R1-R81, 1993.

Martinet, E., F. Luc, E. Rosencher, Ph. Bois, and S. Delaitre, *'Electrical tunability of infrared detectors using compositionally asymmetric GaAs/AlGaAs multi-quantum wells*", Appl. Ph., 60, pp. 92-60, 1992.

Mii, Y. J, R. P. G. Karunasiri, K. L. Wang, M. Chen, and P. F. Yuh, "*Bound-to-extended state absorption GaAs superlattice transport infrared detectors*", Jour. Appl. Phys., 64, pp.
1591-1593,1988.

Mii, Y. J., Wang, K. L., Karunasiri, R. P. G., and Yuh, P. F., *"Observation of large oscillator strengths for both 1-2 and 1-3 inter-su-bband transitions of step quantum wells." J. Appl. Phys.*, **56**, pp. 1046 – 1048, 1990.

Rogalski A., *"Quantum well photoconductors in infrared detector technology"* Journal of Applied Physics Vol 93(8) pp. 4355-4391, (2003).

Touse, Mike, *"Demonstration of a Near and Mid-Infrared Detector Using Multiple Step Quantum Wells",* Master's Thesis, Naval Postgraduate School, Monterey, California, June 2003.

West) L.C. and S.J. Eglash, "*First observation of an extremely large-dipole infrared transition within the conduction band of a GaAs quantum well*", Appl. Phys. Lett., 46, pp. 1156-1158, 1985.

Yu, L.S. and S.S. Li, "*A metal grating coupled bound-to-miniband and transition GaAs multi-quantum well superlattice infrared detector*", Appl. Phys. Lett., 59, pp. 1332-1334, 1991.

Yuh, P.F. and K.L. Wang, "*Optical transitions in a step quantum well*", Jour. Appl. Phys., 65, pp. 4377-4381, 1989.

Zhou, Lifu, *"Fabrication of Quantum Well Detector Array for Thermal Imaging",* Master's Thesis, National University of Singapore, 2001.

THIS PAGE INTENTIONALLY LEFT BLANK

INITIAL DISTRIBUTION LIST

1. Defense Technical Information Center
   Ft. Belvoir, VA

2. Dudley Knox Library
   Naval Postgraduate School
   Monterey, CA

3. Chairman (Code PH)
   Department of Physics
   Naval Postgraduate School
   Monterey, CA

4. Gamani Karunasiri
   Naval Postgraduate School
   Monterey, CA

5. James Luscombe
   Naval Postgraduate School
   Monterey, CA

6. Mihail Giannopoulos
   Xatzidogigou 20
   Larisa 41223, Greece

THIS PAGE INTENTIONALLY LEFT BLANK